



## NRC Publications Archive Archives des publications du CNRC

### Observation of the optical analog of the Mössbauer effect in ruby Szabo, A.

This publication could be one of several versions: author's original, accepted manuscript or the publisher's version. / La version de cette publication peut être l'une des suivantes : la version prépublication de l'auteur, la version acceptée du manuscrit ou la version de l'éditeur.

For the publisher's version, please access the DOI link below. / Pour consulter la version de l'éditeur, utilisez le lien DOI ci-dessous.

#### **Publisher's version / Version de l'éditeur:**

<https://doi.org/10.1103/PhysRevLett.27.323>

*Physical Review Letters*, 27, 6, pp. 323-326, 1971-08

#### **NRC Publications Record / Notice d'Archives des publications de CNRC:**

<https://nrc-publications.canada.ca/eng/view/object/?id=1824391d-582b-45b7-8975-87691db8637>;

<https://publications-cnrc.canada.ca/fra/voir/objet/?id=1824391d-582b-45b7-8975-87691db86373>

Access and use of this website and the material on it are subject to the Terms and Conditions set forth at

<https://nrc-publications.canada.ca/eng/copyright>

READ THESE TERMS AND CONDITIONS CAREFULLY BEFORE USING THIS WEBSITE.

L'accès à ce site Web et l'utilisation de son contenu sont assujettis aux conditions présentées dans le site

<https://publications-cnrc.canada.ca/fra/droits>

LISEZ CES CONDITIONS ATTENTIVEMENT AVANT D'UTILISER CE SITE WEB.

**Questions?** Contact the NRC Publications Archive team at

PublicationsArchive-ArchivesPublications@nrc-cnrc.gc.ca. If you wish to email the authors directly, please see the first page of the publication for their contact information.

**Vous avez des questions?** Nous pouvons vous aider. Pour communiquer directement avec un auteur, consultez la première page de la revue dans laquelle son article a été publié afin de trouver ses coordonnées. Si vous n'arrivez pas à les repérer, communiquez avec nous à PublicationsArchive-ArchivesPublications@nrc-cnrc.gc.ca.



<sup>9</sup>A. C. Nunes, *Acta Crystallogr.*, Sect. A **27**, 219 (1971).

<sup>10</sup>H. Cole, F. Chambers, and H. Dunn, *Acta Crystallogr.* **15**, 138 (1962).

<sup>11</sup>R. M. Moon and C. G. Shull, *Acta Crystallogr.* **17**, 805 (1964).

<sup>12</sup>G. Shirane and V. J. Minkiewicz, *Nucl. Instrum. Methods* **79**, 109 (1970).

<sup>13</sup>*International Tables for X-Ray Crystallography*, edited by C. H. MacGillavry, G. D. Rieck, and K. Lonsdale (Kynock Press, Birmingham, England, 1962), Vol. III, p. 122.

<sup>14</sup>See Ref. 13, Vol. III, p. 233.

<sup>15</sup>M. Born and K. Huang, *Dynamical Theory of Crystal Lattices* (Oxford U. Press, Oxford, England, 1954).

<sup>16</sup>R. A. Cowley, *Advan. Phys.* **12**, 421 (1965).

## Observation of the Optical Analog of the Mössbauer Effect in Ruby

A. Szabo

*National Research Council of Canada, Ottawa, Canada*

(Received 3 May 1971)

Laser-induced fluorescence line narrowing of the ruby  $R_1$  Zeeman spectra at 693.4 nm is reported using a continuous, stable, single-frequency ruby laser for resonant excitation. A resolution in excess of  $10^7$  corresponding to a linewidth of  $\sim 30$  MHz has been achieved. The linewidths are anisotropic with respect to the relative magnetic-field-crystal-axis orientation and, at low Cr concentrations, are expected to be determined by Cr-Al superhyperfine interactions.

There is a close analogy between the recoilless  $\gamma$ -ray transition (Mössbauer effect) and the sharp-line optical fluorescence associated with zero-phonon lines in solids.<sup>1</sup> Both transitions can be termed "zero-phonon" in the sense that the transition occurs with no change in the phonon occupation number, the system terminating in its ground vibrational state. While remarkably high  $Q$ 's have been observed for Mössbauer lines ( $\sim 10^{12}$  in Fe<sup>57</sup>), such values have not yet been observed for optical lines although in principle they should be attainable if the lifetime determines the linewidth. For example, in ruby a  $Q$  value of  $(4 \times 10^{-3})(3 \times 10^{10}/7 \times 10^{-5}) = (\text{lifetime} \times \text{frequency}) \sim 10^{12}$  might be expected for the zero-phonon line. With conventional excitation, such narrow fluorescence lines are not observed because of the inhomogeneous broadening effects of random residual strains.<sup>2</sup> Recently a technique of laser-induced fluorescent line narrowing (FLN) was demonstrated<sup>3</sup> which eliminates inhomogeneous broadening effects. The method consists of observation of the fluorescence following or during resonant excitation of selected ions corresponding to a particular frequency by using a narrow-band laser source. If no spectral diffusion occurs, then the observed fluorescence line shape  $g_{\text{obs}}$  is determined only by homogeneous broadening and consists of a convolution of the homogeneous absorption  $g_a$  and fluorescence  $g_f$  line shapes, i.e.,  $g_{\text{obs}}(\nu) = \int g_a(\nu_L - \nu')g_f(\nu' - \nu) d\nu'$ , where  $\nu_L$  is the laser frequency. Since

the linewidth of the pulsed ruby laser used in earlier work<sup>3</sup> was unknown, quantitative linewidth measurements of the fluorescence were not possible. In this Letter, we describe the use of a continuous, stable, single-frequency ruby laser for excitation which allows continuous observation of the FLN phenomenon. A spectral resolution in excess of  $10^7$  has been achieved corresponding to a linewidth of  $\sim 30$  MHz which is about 100 times narrower than the inhomogeneous width.

The experimental setup, described previously,<sup>3</sup> consisted of a temperature-controlled, piezoelectrically scanned, Fabry-Perot interferometer and a liquid-helium cryostat with optical windows. Two new features were the use of a continuous laser for excitation and the sample-illumination technique. The ruby laser was a 1.5-cm-long rod of 0.03% Cr concentration, which was cooled by conduction to 88°K. We used 1 W of focused 5145-Å light from a Coherent Radiation model 52 argon ion laser for pumping.<sup>4</sup> The gain in the rod was sufficiently high that lasing could easily be achieved with uncoated ends. Oscillation occurred at a single frequency on the  $\bar{E}(\pm \frac{1}{2}) \rightarrow {}^4A_2(\pm \frac{3}{2})$  transition, and this excited the  $\bar{E}(\pm \frac{1}{2}) \rightarrow {}^4A_2(\pm \frac{1}{2})$  lines in the sample. The stability and width of the laser line was better than 5 MHz over  $\sim 100$  sec taken to record spectra; 1 mW of ruby laser light was incident on the surface of the sample at the focus (15 cm) of a lens. The fluorescence light was collimated by the

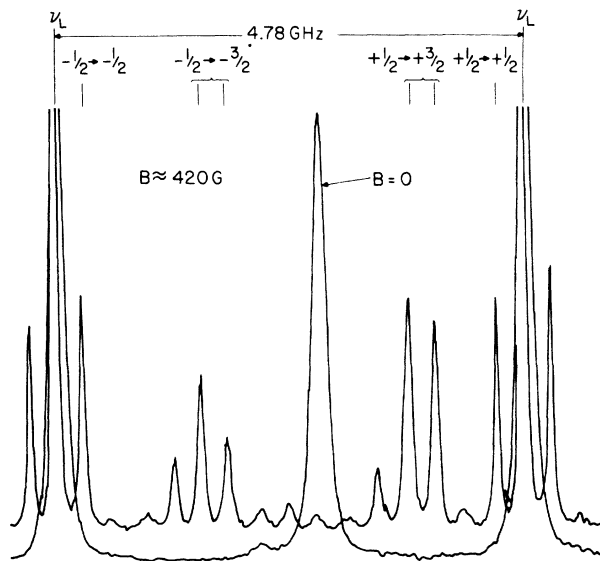


FIG. 1. Zeeman fluorescence spectrum of 0.1% ruby at 4.2°K using single-frequency, resonant ruby-laser excitation ( $E \perp c$ ) in the  $\bar{E}(\pm \frac{1}{2}) \rightarrow {}^4A_2(\pm \frac{1}{2})$  lines. Fabry-Perot free spectral range is 4.78 GHz. Magnetic field orientation to crystal axis is 0°.  $\sigma$  lines are labeled.

same lens and then led into the Fabry-Perot interferometer through a beam splitter. The interferometer has a finesse  $\sim 100$  and approximately a Gaussian line shape determined by irregularities of the plate surfaces.

Some laser-excited Zeeman spectra are shown in Figs. 1-3. We discuss two features of these spectra: (1) the pseudosplitting of the fluorescence lines and (2) the observed linewidths of 30-200 MHz.

For  $\theta = 90^\circ$ , the  $R_1$  Zeeman energy-level scheme is indicated in Fig. 3 as determined by the ground-state<sup>5</sup> and excited-state<sup>6</sup> spin Hamiltonians.

While a three-line fluorescence spectrum might be expected from the energy levels, a six-line spectrum is in fact observed (two lines are superimposed at the laser frequency  $\nu_L$ ). The reason for the line doubling is that two frequency groups are pumped into level 4 because of the overlap of the 3-4 and 2-4 inhomogeneous linewidths. Similar effects are observed for the  $\theta = 0^\circ$  results.

A summary of the experimental line-shape and linewidth data is given in Table I. The broadening is similar to that observed in the ground-state<sup>7</sup> and excited-state<sup>6,8</sup> EPR of ruby and aris-es, at least in part, from the superhyperfine interactions between the  $\text{Cr}^{3+}$  and the thirteen nearest-neighbor Al nuclear spins. At  $\theta = 0^\circ$  ( $B = 0$ ), Gaussian line shapes (Fig. 2) are observed as ex-

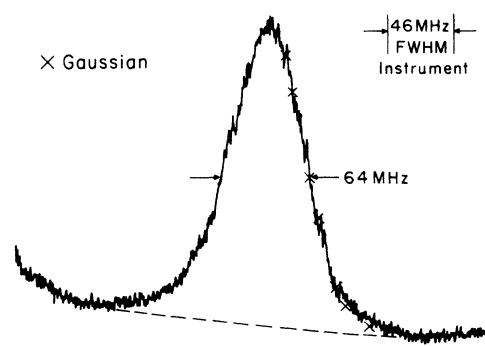


FIG. 2. Expanded view of the  $\bar{E}(-\frac{1}{2}) \rightarrow {}^4A_2(-\frac{1}{2})$  fluorescence line in Fig. 1 showing its Gaussian shape.

pected from the superhyperfine broadening mechanism.<sup>7</sup> On the other hand at  $\theta = 90^\circ$  (Fig. 3) or for  $B = 0$ , the line shapes markedly depart from Gaussian and are well described by a Lorentz-Gaussian (Voigt) shape.

A simple explanation of the linewidth  $\theta$  and transition dependence is possible using a model developed for a description of photon-echo behavior<sup>9</sup> in which the Al nuclear spins are considered to produce a random, time-varying field  $\Delta B$  at the Cr site. Considering quantities such as  $\partial\nu/\partial B$  and  $\partial\nu/\partial\theta$ , we expect narrower linewidths at  $\theta = 0^\circ$  since here  $\partial\nu/\partial\theta = 0$ . Also, at  $\theta = 0^\circ$ ,  $\partial\nu/\partial B$  is smaller for  $\bar{E}(\pm \frac{1}{2}) \rightarrow {}^4A_2(\pm \frac{1}{2})$  than for  $\bar{E}(\pm \frac{1}{2}) \rightarrow {}^4A_2(\pm \frac{3}{2})$  in agreement with observa-

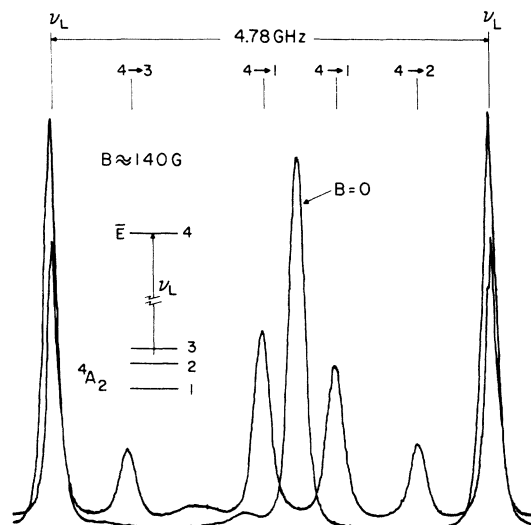


FIG. 3. Zeeman fluorescence spectrum of 0.1% ruby at 4.2°K using single-frequency, resonant ruby-laser excitation ( $E \perp c$ ) in the  $\bar{E}(\pm \frac{1}{2}) \rightarrow {}^4A_2(\pm \frac{1}{2})$  lines. Fabry-Perot free spectral range is 4.78 GHz. Magnetic field orientation to crystal axis is  $90^\circ$ . Inset shows splitting of  $R_1$  levels.

TABLE I. Ruby fluorescence line shapes and linewidths at 4.2°K obtained by resonant ruby-laser excitation.

Angle	Magnetic field (G)	Transition ( $\bar{E} \rightarrow {}^4A_2$ )	$\Delta_{\text{obs}}$ = observed FWHM linewidth (MHz)	$\Delta$ = deconvoluted FWHM linewidth <sup>a</sup> (MHz)	Line shape
•••	0	All	180 ± 10	•••	Voigt
0°	420	$\pm \frac{1}{2} \rightarrow \pm \frac{1}{2}$	64 ± 5	32 $^{+7}_{-11}$	Gaussian
0°	420	$\pm \frac{1}{2} \rightarrow \pm \frac{3}{2}$	81 ± 5	59 $^{+14}_{-18}$	Gaussian
90°	140	All	180 ± 10	•••	Voigt

<sup>a</sup> Assuming  $\Delta(-\frac{1}{2}, -\frac{1}{2}) = \Delta(+\frac{1}{2}, +\frac{1}{2})$  and  $\Delta(-\frac{1}{2}, -\frac{3}{2}) = \Delta(+\frac{1}{2}, +\frac{3}{2})$ .

tions. Taking<sup>5</sup>  $\Delta B_z = 7$  G, we calculate at  $\theta = 0^\circ$  the homogeneous linewidths  $\Delta(\pm \frac{1}{2}, \frac{3}{2}) = 35$  MHz.

A more precise description of hyperfine broadening of the  $R_1$  lines in ruby is possible using a modification of Wenzel's theory<sup>7</sup> of ground-state broadening. In the high-field approximation in which the nuclear spin is quantized along the magnetic field, we derive from Wenzel's Eq. (24) the second moment  $\langle \Delta E^2 \rangle$  of the  $R_1$  transitions at  $\theta = 0^\circ$ :

$$\langle \Delta E^2 \rangle = \frac{1}{3} I(I+1) \sum_i [A_i^* \langle S_z^* \rangle - A_i \langle S_z \rangle + (B_i^* \langle S_z^* \rangle - B_i \langle S_z \rangle) n_{zi}]^2. \quad (1)$$

Here  $n_{zi}$  is the component along the optic axis of the unit vector  $\hat{n}$  along the Cr-Al direction, and starred quantities refer to excited-state interaction coefficients which appear in the effective nuclear spin Hamiltonian for the  $i$ th Al,

$$H_i(\text{excited state}) = A_i^* \langle \bar{S}^* \rangle \cdot \bar{I} + B_i^* \langle \bar{S}^* \rangle \cdot \bar{n}_i \bar{I} \cdot \bar{n}_i + (\gamma/I) \bar{I}_i \cdot \bar{H} + Q_i^* I_{zi}^2, \quad (2)$$

with a similar equation for  $H_i(\text{ground state})$ . In Eq. (2),  $A_i^*$  and  $B_i^*$  are appropriate combinations of contact and dipolar Cr-Al interaction coefficients (ground-state values of  $A_i$ ,  $B_i$ , and  $Q_i$  are tabulated in Ref. 7),  $\langle S^* \rangle$  is the electron spin expectation value,  $Q_i^*$  is the quadrupole coefficient,  $\gamma$  is the nuclear moment, and  $I = \frac{5}{2}$ . To permit calculations of  $\langle \Delta E^2 \rangle$  in Eq. (1) we have neglected  $Q_i$ 's and have assumed that  $B_i^* \equiv k B_i = (g_{11}^*/g_{11}) B_i$  (point-dipole approximation). Also,  $A_i^* = f A_i + (f-k) B_i/3$ , where  $f$  is the ratio of excited- to ground-state contact interaction constants. Following Ref. 9, we took  $f = 1.4$  for  $\bar{E}(+\frac{1}{2})$  and  $f = 0.8$  for  $\bar{E}(-\frac{1}{2})$ . Assuming a Gaussian line shape, we calculated the following full width at half-maximum (FWHM) linewidths:  $\Delta(-\frac{1}{2}, -\frac{1}{2}) = 4.0$  MHz,  $\Delta(+\frac{1}{2}, +\frac{1}{2}) = 6.4$  MHz,  $\Delta(+\frac{1}{2}, +\frac{3}{2}) = 28$  MHz, and  $\Delta(-\frac{1}{2}, -\frac{3}{2}) = 35$  MHz. These widths are in fair agreement with values calculated from the simple model described earlier. The four distinct linewidths will produce five distinct observed (remote from  $\nu_L$ ) fluorescence linewidths each consisting of a convolution of instrument, absorption, and fluorescence line shapes. Thus, for example, one of the observed  $\bar{E}(+\frac{1}{2}) \rightarrow {}^4A_2(+\frac{3}{2})$  lines in Fig. 1 has a width

$$\Delta_{\text{obs}}(+\frac{1}{2}, +\frac{3}{2}) = [\Delta_{\text{inst}}^2 + \Delta^2(-\frac{1}{2}, -\frac{1}{2}) + \Delta^2(+\frac{1}{2}, +\frac{3}{2})]^{1/2},$$

as determined by excitation in the  $\bar{E}(-\frac{1}{2}) \rightarrow {}^4A_2(-\frac{1}{2})$  transition and fluorescence in  $\bar{E}(+\frac{1}{2}) \rightarrow {}^4A_2(+\frac{3}{2})$  with  $\bar{E}(+\frac{1}{2})$  populated by Orbach relaxation<sup>8</sup> in  ${}^2E$ . Unfortunately the precision available from the present experimental setup (determined by vibrations, pump-power fluctuations, etc.) did not permit consistent measurement of the small linewidth differences suggested by theory (the linewidths in Table I are average values over all the lines). It is clear however that the measured widths are larger than the theoretical values, in particular for  $\Delta(\pm \frac{1}{2}, \pm \frac{1}{2})$ . This may be because of a failure of the high-field approximation in the present, relatively low-field case; imprecise knowledge of the excited-state interaction coefficients; or Cr-Cr interaction broadening.<sup>10</sup> Calculations indicate that phonon broadening due to Raman<sup>11</sup> and direct processes<sup>12</sup> in  ${}^2E$  is negligible at 4.2°K. Decrease of the excitation energy by a factor 10 produced no change in linewidth, indicating that saturation broadening was not a factor.<sup>13</sup>

In summary, a technique which permits continuous observation of optical spectra of solids without the inhomogeneous broadening effects of random strains has been demonstrated. The technique should be applicable to other materials

using narrow-band, cw, tunable dye lasers or parametric oscillators. While  $Q$  values considerably smaller than that given by lifetime were obtained for ruby, much larger values are expected for suitable ion-host combinations. By restricting the direction of observation along the laser beam, the FLN technique is also expected to apply to gases in a manner similar to that described previously<sup>14</sup> for a sequence of laser action and fluorescence. An advantage of FLN homogeneous linewidth observation over nonlinear absorption techniques<sup>15</sup> is that many lines can be observed without tuning the laser. There are, of course, corresponding disadvantages, e.g., much spectral confusion when many overlapping lines are excited. The task of fine frequency control is now transferred to the detection system; thus, for example, we have the delightful prospect of observation of hyperfine, Zeeman, Stark, or stress spectra by heterodyne methods.

The author wishes to acknowledge with thanks the help of L. E. Erickson in constructing the equipment, the technical assistance of E. L. Dimock, and a useful encounter with G. R. Hanes at a critical point in the experiments.

<sup>1</sup>R. H. Silsbee, in *Optical Properties of Solids*, edited by S. Nudelman and S. S. Mitra (Plenum, New York, 1969), p. 607.

<sup>2</sup>A. M. Stoneham, *Rev. Mod. Phys.* **41**, 82 (1969).

<sup>3</sup>A. Szabo, *Phys. Rev. Lett.* **25**, 924 (1970).

<sup>4</sup>M. Birnbaum, P. H. Wenzikowski, and C. L. Fincher, *Appl. Phys. Lett.* **16**, 436 (1970).

<sup>5</sup>N. Laurance, E. C. McIrvine, and J. Lambe, *J. Phys. Chem. Solids* **23**, 515 (1962).

<sup>6</sup>S. Geschwind, G. E. Devlin, R. L. Cohen, and S. R. Chinn, *Phys. Rev.* **137**, A1087 (1965).

<sup>7</sup>R. F. Wenzel, *Phys. Rev. B* **1**, 3109 (1970).

<sup>8</sup>T. Muramoto, Y. Fukuda, and T. Hashi, *J. Phys. Soc. Jap.* **26**, 1551 (1969).

<sup>9</sup>D. Grischkowsky and S. R. Hartmann, *Phys. Rev. B* **2**, 60 (1970).

<sup>10</sup>W. J. C. Grant and M. W. P. Strandberg, *Phys. Rev.* **135**, A727 (1964).

<sup>11</sup>D. E. McCumber and M. D. Sturge, *J. Appl. Phys.* **34**, 1682 (1963).

<sup>12</sup>N. A. Kurnitt, I. D. Abella, and S. R. Hartmann, in *Physics of Quantum Electronics*, edited by P. L. Kelley, B. Lax, and P. E. Tannenwald (McGraw-Hill, New York, 1966), p. 267.

<sup>13</sup>There is however a dramatic apparent saturation effect when the passage of the laser beam through the crystal is viewed transversely. As the beam is focused down, the penetration increases from  $< 1$  mm for a wide beam to over the entire sample length of 4 mm for a focused beam. The "saturation" occurs because of the net transfer of ions from the  $(\pm \frac{1}{2})$   $^4A_2$  levels to the  $(\pm \frac{3}{2})$   $^4A_2$  levels produced by optical-pumping effects similar to that in gases. The governing factors are the fluorescence lifetime (4 msec), the  $^4A_2$  spin-lattice relaxation time ( $\sim 200$  msec at 4.2°K), and the spin-spin cross relaxation time in  $^4A_2$ .

<sup>14</sup>W. G. Schweitzer, Jr., M. M. Birky, and J. A. White, *J. Opt. Soc. Amer.* **57**, 1226 (1967).

<sup>15</sup>G. R. Hanes and C. E. Dahlstrom, *Appl. Phys. Lett.* **14**, 362 (1969).

## Band-Structure Effects in Metal-GaSb Tunnel Contacts Under Pressure\*

P. Guétin and G. Schröder

*Laboratoires d'Electronique et de Physique appliquée, 94 Limeil-Brevannes, France*

(Received 30 April 1971)

Tunneling at 4.2°K from lead into degenerate  $n$ -type GaSb under hydrostatic pressure exhibits huge changes when conduction-band extrema cross each other. In the indirect-gap configuration, strong phonon-assisted structures show up together with a typical resistance kink related to the onset of a (000) tunneling path. The measured interband pressure coefficient is  $-9.6$  meV/kbar. All results suggest that the band crossing occurs 3 kbar higher than expected.

Tunneling measurements in metal-GaSb contacts under hydrostatic pressure exhibit strong effects which are definitely due to the crossing of the  $\Gamma$  (000) and  $L$  (111) conduction-band extrema. Although band-structure effects in tunnel heterojunctions have previously been reported in the literature,<sup>1-4</sup> this work gives, to our knowledge, the first unambiguous quantitative

results concerning externally controlled band-structure effects in such junctions. Gallium antimonide is especially well suited for a systematic study of the tunnel mechanisms involved in direct- and indirect-gap semiconductors: The interband energy separation  $E_L - E_\Gamma$  can be changed in both amplitude and sign by reasonably low pressure. GaSb is a direct-gap semiconductor<sup>5</sup>